JACS
JOURNAL OF THE AMERICAN CHEMICAL SOCIETY
Article
pubs.acs.org/JACS

Large Tunneling Effect on the Hydrogen Transfer in Bis(μ-oxo)dicopper Enzyme: A Theoretical Study

Kisoo Park,[†] Youngshang Pak,*[,‡] and Yongho Kim*[,†]

[†]Department of Applied Chemistry, Kyung Hee University, 1 Seochun-Dong, Giheung-Gu, Yongin-Si, Gyeonggi-Do 446-701, Korea
[‡]Department of Chemistry and Institute of Functional Materials, Pusan National University, Busan 609-735, Korea

Supporting Information

ABSTRACT: Type-III copper-containing enzymes have dicopper centers in their active sites and exhibit a novel capacity for activating aliphatic C−H bonds in various substrates by taking molecular oxygen. Dicopper enzyme models developed by Tolman and co-workers reveal exceptionally large kinetic isotope effects (KIEs) for the hydrogen transfer process, indicating a significant tunneling effect. In this work, we demonstrate that variational transition state theory allows accurate prediction of the KIEs and Arrhenius parameters for such model systems. This includes multidimensional tunneling based on state-of-the-art quantum-mechanical calculations of the minimum-energy path (MEP). The computational model of bis(μ-oxo)dicopper enzyme consists of 70 atoms, resulting in a 204-dimensional potential energy surface. The calculated values of $E_a^H - E_a^D$, A_H/A_D, and the KIE at 233 K are −1.86 kcal/mol, 0.51, and 28.1, respectively, for the isopropyl ligand system. These values agree very well with experimental values within the limits of experimental error. For the representative tunneling path (RTP) at 233 K, the pre- and post-tunneling configurations are 3.3 kcal/mol below the adiabatic energy maximum, where the hydrogen travels 0.54 Å by tunneling. We found that tunneling is very efficient for hydrogen transfer and that the RTP is very different from the MEP. It is mainly heavy atoms that move as the reaction proceeds from the reactant complex to the pretunneling configuration, and the hydrogen atom suddenly hops at that point.

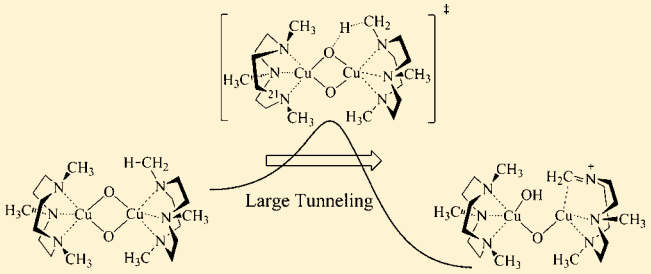

1. INTRODUCTION

Because they catalytically activate molecular oxygen, copper-containing metalloenzymes play an important role in many biological processes.[1−3] Type-III copper-containing enzymes, including catechol oxidase, hemocyanins, and tyrosinase, have a dicopper center in their active sites. These enzymes exhibit the novel ability to activate aliphatic C−H bonds by taking molecular oxygen. They have received considerable attention because of their ability to oxidize organic substrates. One way to study the catalytic activity of these enzymatic reactions is to design comprehensive model systems by reducing the structural complexity of the biological enzymes. Tolman and co-workers[4] synthesized a bicopper model complex that mimics the biological functions of type-III copper-containing enzymes. They extensively characterized its catalytic activity and the mechanistic pathways by which it converts organic substrates into their oxidized forms. This model complex is made of two pairs of alternately linked oxygen and copper atoms that form a Cu_2O_2 core. The experimentally observed Cu−O bond length is 1.81 Å, and the Cu−O−Cu and O−Cu−O angles are 101.4 and 78.6°, respectively. Three nitrogen atoms are coordinated to copper and connected by $-CH_2CH_2-$ chains. The organic substrates for the C−H activation are also chemically bonded to the nitrogen atom. Tolman and co-workers[4] successfully developed two copper model systems using an isopropyl or benzyl group as the aliphatic substrate. They found that the C−H activation process was initiated by the transfer of a hydrogen atom from the aliphatic carbon of the aliphatic substrate. The reaction mechanism of the hydrogen transfer is depicted in Figure 1. The first step of the reaction is the rate-determining step. In this step, the hydrogen atom is transferred to an oxygen in the Cu_2O_2 core, and the ring subsequently opens. In the second step, the resulting OH is re-bound to the isopropyl or benzyl group.

The most striking observation during the hydrogen transfer that triggers C−H bond activation was the unusually large H/D kinetic isotope effect (KIE). The KIE values for the benzyl and isopropyl substrates were 40 and 26 at 233 K, respectively. This implies a significant quantum-mechanical tunneling effect in the rate-determining step. A large KIE value of 22 was also observed for the alcohol oxidation of galactose oxidase (monocopper enzyme).[5] Substantial quantum-mechanical tunneling appears to be a key factor in characterizing the hydrogen transfer kinetics of many of the oxidation reactions of various copper enzymes.[6] A more realistic description of the quantum-mechanical tunneling effect is required in order to determine any valid theoretical predictions of the hydrogen transfer reaction in copper enzyme model systems. Previous theoretical studies[7,8] used a hybrid quantum mechanics (QM)/

Received: November 25, 2011
Published: January 24, 2012

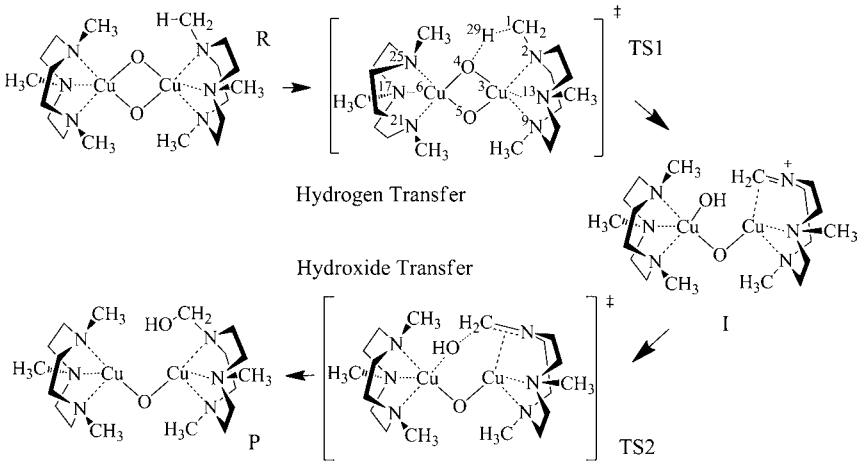

Figure 1. Reaction mechanism for hydrogen transfer.

molecular mechanics (MM) method. These studies investigated the structures of stationary points (reactant, transition state, and product), the energetics of the hydrogen transfer, and the KIE values. The mechanistic interpretation based on QM/MM seems reasonable and consistent with experimental observation. However, the enthalpy of activation was too small, and the predicted KIEs were smaller than the experimental values by a factor of 2. They used a simple one-dimensional tunneling approximation based on the imaginary frequencies of transition states, which greatly underestimated the tunneling probabilities and gave smaller KIEs. More importantly, the predicted KIEs of the methyl ligand system were larger than those of the benzyl ligand system,[8] which contradicts the experimental results. Advanced schemes that more accurately account for the tunneling effect should be applied.

In this work, potential and vibrationally adiabatic ground-state energies were calculated along the intrinsic reaction coordinate. These values were used to calculate the rate constants for the hydrogen transfer in Tolman's dicopper enzyme model system. Variational transition state theory including a multidimensional semiclassical tunneling scheme was used.[9−14] The KIEs were also calculated. This method is more realistic because the hydrogen transfer kinetics can be more precisely described on the well-defined multidimensional potential energy landscapes. For this purpose, the present work involves a full range of QM calculations to determine the intrinsic reaction path of the hydrogen transfer. In addition, rate calculations were performed using variational transition state theory including tunneling. Although Tolman's model system is a much reduced version of real dicopper enzymes, it is still too large for full quantum-mechanical reaction path calculations. Therefore, we further reduced its size by replacing the alkyl substrate with a methyl group. This resulted in a total of 70 atoms, giving a 204-dimensional potential energy surface.

2. COMPUTATIONAL DETAILS

For the model system of 70 atoms, stationary points were calculated with the density functional methods B3LYP,[15] M06,[16] M06-L,[17] M06-2X,[16] and PBEPBE.[18] The LANL2DZ[19] basis set with an effective core potential was always used for copper, which will not be mentioned in this paper. The 6-31G(d,p) and D95V[20] basis sets were used for C, H, O, and N atoms. Each minimum and transition state (TS) was confirmed to have zero and one imaginary frequency, respectively. The M06 density functional was used for the rate calculation because it has given good benchmark results for metal complexes.[16,21] For structures, energies, and Hessians along the minimum energy path (MEP) that were required for rate calculations including the tunneling effect, the basis set size was reduced by using a 6-31G(d,p)/D95V mixed basis set, in which the 6-31G(d,p) basis set was used for O and the reacting methyl group and the D95V basis set was used for all other atoms.

The reaction rates were calculated using variational transition state theory including a transmission coefficient[9−14] that accounts for multidimensional tunneling. All of the rate calculations were carried out by direct dynamics[22] with the interpolated variational transition state theory by mapping[23] (IVTST-M) algorithm. This was done using the Gaussrate program,[24] which is an interface of Gaussian 03[25] and the Polyrate dynamics program.[26] The MEP corresponds to the path of steepest descent in isoinertial coordinates on a $(3N - 6)$-dimensional potential energy surface. The signed distance from the TS along the MEP in isoinertial coordinates is called the reaction coordinate, s. The MEP for each of the isotopomers was obtained using the RODS algorithm.[27,28] The variational transition state for a canonical ensemble at temperature T is located at the point on the MEP where the generalized free energy of activation is a maximum. All vibrational energies and vibrational free energies were computed harmonically from frequencies. This yielded the canonical variational theory (CVT) rate constant, given by[10,13]

$$k^{\mathrm{CVT}} = \min_{s} k^{\mathrm{GT}}(T, s) = \frac{k_{\mathrm{B}}T}{h}\frac{Q^{\mathrm{GT}}(T, s_*^{\mathrm{CVT}})}{Q^{\mathrm{R}}} \exp\left[-\Delta V_{\mathrm{MEP}}(s_*^{\mathrm{CVT}})/k_{\mathrm{B}}T\right] \quad (1)$$

where the superscript GT denotes generalized transition state theory, k_{B} is Boltzmann's constant, h is Planck's constant, s_*^{CVT} is the value of s at which k^{GT} is minimized (the location of the canonical variational transition state), and Q^{GT} and Q^{R} are partition functions for the generalized transition state and reactants, respectively. In order to include tunneling, $k^{\mathrm{CVT}}(T)$ is multiplied by a transmission coefficient, $\kappa^{\mathrm{CVT/G}}$:

$$k^{\mathrm{CVT/G}}(T) = \kappa^{\mathrm{CVT/G}}(T)k^{\mathrm{CVT}}(T) \quad (2)$$

The transmission coefficient is defined as the ratio of the thermal average of the quantal transmission probability $P^{\mathrm{G}}(E)$ to the thermal average of the classical transmission probability for the effective vibrationally adiabatic potential energy along the reaction coordinate that is implied by CVT theory, $P_{\mathrm{C}}^{\mathrm{CVT/G}}(E)$:[9,10,14]

$$\kappa^{\mathrm{CVT/G}}(T) = \frac{\int_0^\infty P^{\mathrm{G}}(E)\exp(-E/k_{\mathrm{B}}T)\,\mathrm{d}E}{\int_0^\infty P_{\mathrm{C}}^{\mathrm{CVT/G}}(E)\exp(-E/k_{\mathrm{B}}T)\,\mathrm{d}E} \quad (3)$$

dx.doi.org/10.1021/ja211073t | J. Am. Chem. Soc. 2012, 134, 3524−3531

Table 1. Signed Errors and Mean Unsigned Errors (MUEs) for Reactant Geometric Parameters with Respect to Experimental Values (Å)

computational level	r(Cu−Cu)	r(O−O)	r(Cu−O)$_{av}$ [a]	r(^{6}Cu−^{21}N)	r(^{6}Cu−^{25}N)	r(^{6}Cu−^{17}N)	MUE
B3LYP/6-31G(d,p)	0.022	0.030	0.017	0.027	0.032	0.152	0.047
B3LYP/D95V	0.088	0.061	0.053	0.020	0.019	0.098	0.057
M06/6-31G(d,p)	−0.034	0.046	0.001	−0.010	−0.002	0.083	0.029
M06/D95V	0.035	0.069	0.035	−0.022	−0.015	0.059	0.039
M06/6-31G(d,p)/D95V	−0.020	0.039	0.004	−0.019	−0.014	0.076	0.029
M06-L/6-31G(d,p)	−0.016	0.097	0.025	0.011	0.024	0.081	0.042
M06-L/D95V	0.050	0.124	0.058	0.004	0.009	0.036	0.047
PBEPBE/6-31G(d,p)	0.047	0.070	0.040	0.033	0.033	0.136	0.060
PBEPBE/D95V	0.118	0.096	0.076	0.020	0.029	0.087	0.071
MPW1K/ECP(+)/UFF [b]	0.066	−0.049	0.006				
exptl [c]	2.794	2.287	1.806	1.986	1.987	2.298	

[a] Average of four Cu−O bond lengths. [b] Reference 8. [c] Reference 34.

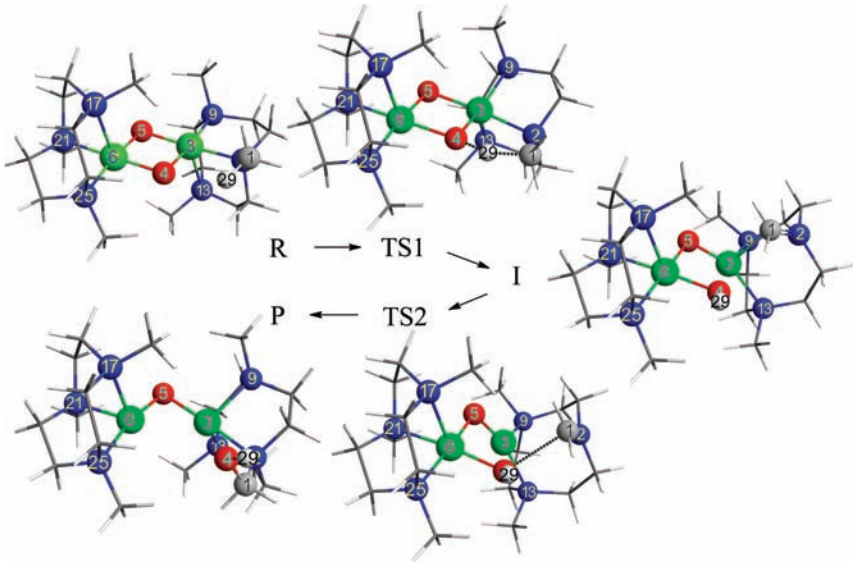

Figure 2. Optimized structures of the reactant (R), first transition state (TS1), intermediate (I), second transition state (TS2), and product (P) at the M06/6-31G(d,p)/D95V level. The ligand system bound to the left side of ^{6}Cu was set as a datum structure to ensure a consistent viewing angle because it was hardly changed in the reaction.

Since the value of $P_C^{CVT/G}(E)$ is unity above the threshold energy of the CVT calculations and zero below it, eq 3 reduces to

$$\kappa^{CVT/G}(T) = \frac{1}{k_B T} e^{V_a^G(s_*^{CVT})/k_B T} \int_0^\infty P^G(E) e^{-E/k_B T}\, dE \quad (4)$$

which can be written as

$$\kappa^{CVT/G}(T) = \frac{1}{k_B T} \kappa^{CVT/CAG} \int_0^\infty \left[P^G(E) e^{V^{AG}/k_B T}\right] e^{-E/k_B T}\, dE \quad (5)$$

where

$$\kappa^{CVT/CAG} = e^{[V_a^G(s_*^{CVT}) - V^{AG}]/k_B T} \quad (6)$$

$V_a^G(s_*^{CVT})$ is the ground-state adiabatic energy barrier evaluated at the canonical variational transition state, and V^{AG} is defined by

$$V^{AG} = \max_s V_a^G(s) \quad (7)$$

The centrifugal-dominant small-curvature semiclassical adiabatic ground state (CD-SCSAG) tunneling approximation[11] was used to calculate $P^G(E)$. This is called small-curvature tunneling (SCT).

In the IVTST-M algorithm, the information necessary for the CVT/SCT calculation (energies, gradients, and Hessians) is computed at a small number of points along the MEP and fitted to spline functions under tension. In this study, 799 energies and gradients (at every 0.001 Å in the region −0.16 Å ≤ s ≤ 0.1 Å and every 0.005 Å in the regions −0.755 < s < −0.16 and 0.1 Å < s < 2.16 Å) along the MEP and 13 Hessians (at s = −0.6, −0.4, −0.2, −0.1, 0.15, 0.25, 0.60, 1.00, 1.20, 1.40 Å, reactant, product, and TS) were used.

3. RESULTS AND DISCUSSION

3.1. Structural Changes in the Hydrogen and Hydroxyl Transfer Reactions. Several geometric parameters (four Cu−O bond lengths, six Cu−N bond lengths, the Cu−Cu distance, and the O−O distance) of reactants optimized using various DFT methods were compared with the experimental values. The results are listed in Table 1. At all DFT levels used, the 6-31G(d,p) basis set resulted in better agreement with experimental values than did the D95V basis set. The M06 level that used the 6-31G(d,p) and 6-31G(d,p)/D95V basis sets produced the smallest mean unsigned error (MUE) in the geometric parameters when compared with experimental values. This mixed basis set was used to generate potential energy curves for the hydrogen transfer reaction and

dx.doi.org/10.1021/ja211073t | J. Am. Chem. Soc. 2012, 134, 3524−3531

to calculate rates and KIEs including tunneling. Figure 2 shows the optimized structures of the reactant (R), the transition state for the hydrogen transfer (TS1), the intermediate (I), the transition state for the hydroxide transfer (TS2), and the product (P) calculated at the M06/6-31G(d,p)/D95V level. Several geometric parameters for the stationary points (R, TS1, I, TS2, and P) that were optimized at the M06/6-31G(d,p)/D95V level are listed in Table 2. The average ^{6}Cu−N distances for all stationary points were almost the same, which strongly suggests that the ligand system bound to ^{6}Cu hardly changed during the reaction. The average ^{3}Cu−N distances in R and P were similar. Therefore, the ligand systems bound to the two copper atoms remained nearly intact at R and P. The ^{3}Cu−^{6}Cu distance in the product became smaller, which is probably due to breaking of the diamond core. The major structural changes from R to TS1 occurred in the ^{1}C−^{29}H and ^{4}O−^{29}H bonds that are broken and formed in the hydrogen transfer reaction and also in the ^{1}C−^{4}O distance that brings the methyl group closer to the Cu_2O_2 core. The ^{1}C−^{2}N bond became slightly shorter because of the increased double bond character resulting from partial ^{1}C−^{29}H bond breaking at the TS. Otherwise, there were no significant structural deformations.

Table 2. Selected Geometric Parameters of TS1, I, TS2, and P Calculated at the M06/6-31G(d,p)/D95V Level[a]

	R	TS1	I	TS2	P
$r(^{3}Cu-^{6}Cu)$	2.774	2.843	3.073	2.989	2.595
$r(^{4}O-^{5}O)$	2.326	2.367	2.575	2.592	
$r(^{3}Cu-N)_{av}$[b]	2.103	2.085	2.312	2.288	2.096
$r(^{6}Cu-N)_{av}$[c]	2.105	2.103	2.143	2.147	2.095
$r(^{1}C-^{29}H)$	1.092	1.345	3.567		
$r(^{4}O-^{29}H)$	2.370	1.197	0.965		
$r(^{1}C-^{4}O)$	2.904	2.405	2.921	2.560	1.390
$r(^{1}C-^{2}N)$	1.483	1.434	1.316	1.297	1.485
$r(^{3}Cu-^{4}O)$	1.807	1.857	2.800		
$r(^{6}Cu-^{4}O)$	1.807	1.898	1.858	1.885	3.755
$r(^{3}Cu-^{1}C)$	2.857	2.789	2.189	2.778	2.899
ϕ[d]	170	174	91	92	174
φ[e]	180	176	147	133	

[a]Bond lengths are in Å and angles in deg. [b]Average of three ^{3}Cu−N distances. [c]Average of three ^{6}Cu−N distances. [d] ^{5}O−^{6}Cu−^{3}Cu−^{2}N dihedral angle. [e] ^{6}Cu−^{5}O−^{4}O−^{3}Cu dihedral angle.

Several significant structural changes occurred with the change from TS1 to I. The average ^{3}Cu−N distance increased, the dihedral angles ^{5}O−^{6}Cu−^{3}Cu−^{2}N (ϕ) and ^{6}Cu−^{5}O−^{4}O−^{3}Cu (φ) changed significantly, and the ^{3}Cu−^{4}O and ^{3}Cu−^{1}C bonds were broken and formed, respectively. The hydrogen transfer from ^{1}C to ^{4}O results in breaking of the ^{3}Cu−^{4}O bond and formation of the ^{1}C−^{2}N double bond (its bond length became 1.316 Å at I). The dihedral angle φ represents the folding of two triangles (^{6}Cu−^{4}O−^{5}O and ^{3}Cu−^{4}O−^{5}O) to form the diamond structure of the Cu_2O_2 core. The dihedral angle ϕ represents the torsion of the ^{2}N atom (and the whole ligand system bound to ^{3}Cu) along the ^{6}Cu−^{3}Cu axis with respect to the ^{5}O−^{6}Cu−^{3}Cu plane. The folding angle φ is 180° for the reactant. The diamond core was broken with the ^{3}Cu−^{4}O bond, which may have resulted in the smaller φ value for the intermediate. Interestingly, the torsion angle ϕ changed from 170° in the reactant to 91° in the intermediate. This means that the ligand system bound to ^{3}Cu twisted clockwise by ∼80° during the hydrogen transfer reaction. The folding of the diamond core and the twisting of the ligand system bound to ^{3}Cu occurred simultaneously with the hydrogen transfer. This resulted in an increased average ^{3}Cu−N distance. More importantly, the ^{3}Cu−^{1}C distance greatly decreased (2.189 Å), becoming even smaller than the ^{3}Cu−^{2}N distance (2.616 Å). As a result, a bond formed between copper and the methylene carbon of ^{1}C═^{2}N. The Mulliken partial charges of the ^{2}N atom at R, TS, and I were −0.31, −0.22, and 0.01, respectively, whereas those of ^{3}Cu were 0.59, 0.52, and 0.24, respectively. The double-bond character in ^{1}C−^{2}N results from formation of a π bond by the nonbonding nitrogen electron. This increases the partial charge of the ^{2}N atom, which produces a Coulomb repulsion with copper. In addition, coordination of the ^{2}N atom to copper is geometrically unfavorable because of increased planarity at the ^{2}N center. Instead, the π electron on the methylene carbon forms a strong coordination bond to copper.

When the reaction goes from I to TS2, the hydroxyl group is transferred, with the ^{3}Cu−^{1}C distance increasing to 2.778 Å, the twisting angle ϕ remaining the same, and the folding angle φ decreasing slightly. The ^{6}Cu−^{4}O distance increased by only 0.03 Å, while the ^{1}C−^{4}O distance decreased by 0.36 Å (from 2.921 Å at I to 2.560 Å at TS2). These results suggest that the TS2 structure is reached very early along the reaction coordinate of the hydroxyl transfer and that the major structural change involves the heavy-atom motion that brings the reaction center closer. The chemical bond hardly changes. From TS2 to P, major structural changes were made in the ligand systems, which became similar to their original structures in the reactant. The twisting angle ϕ and the average Cu−N distances became similar to those in the reactant, meaning that the ligand system bound to ^{3}Cu is twisted (counterclockwise) back to its original structure. The ^{1}C−^{4}O and ^{1}C−^{2}N bonds became shorter and longer, respectively, as a result of the hydroxyl transfer.

3.2. Energetics of the Hydrogen and Hydroxyl Transfer Reactions. Table 3 lists the relative potential energies of the stationary points with respect to the reactant at various DFT levels. Overall, the M06 level tended to have a higher potential energy barrier for the hydrogen transfer, whereas the PBEPBE and MPW1K levels had much lower barriers. The potential energy barrier at the M06/6-31G(d,p)/D95V level was 23.8 kcal/mol, which is slightly larger than the value at the same level when the 6-31G(d,p) basis set was used. The potential energies of the intermediate depended on the

Table 3. Relative Potential Energies (kcal/mol) for Stationary Points (TS1, I, TS2, and P) with Respect to the Reactant

method	TS1	I	TS2	P
B3LYP/6-31G(d,p)	18.2	−14.7	−5.53	−36.7
B3LYP/D95V	16.8	−6.26	2.05	−21.9
M06/6-31G(d,p)	19.5	−18.6	−13.98	−46.7
M06/D95V	21.8	−5.44	0.98	−26.0
M06/6-31G(d,p)/D95V	23.8	−11.2	−5.95	−41.2
M06-L/6-31G(d,p)	19.3	−8.56	−0.19	−27.3
M06-L/D95V	19.4	−0.09	10.8	−10.0
PBEPBE/6-31G(d,p)	12.9	−11.9		
PBEPBE/D95V	12.8	−3.3		
MPW1K/ECP(+)/UFF[a]	12.9	−17.0		

[a]Reference 8.

dx.doi.org/10.1021/ja211073t | J. Am. Chem. Soc. 2012, 134, 3524−3531

computational level and the size of the basis sets. The reaction energies for the hydrogen transfer (the relative energies of the intermediate in Table 3) became more negative as the size of the basis set increased, meaning that larger basis sets tended to yield greater exoergicities for the reactions. It is interesting that the M06/6-31G(d,p) and MPW1K levels predicted very similar exoergicities for the hydrogen transfer reaction. The M06/6-31G(d,p)/D95V level predicted a slightly smaller exoergicity. The differences in the relative energies of I and TS2 give the barrier heights of the second step, in which the hydroxide is rebound to the methylene carbon to make an alcohol group. The hydroxylation reaction barriers were in the range of 4.62 and 10.9 kcal/mol, and the former and the latter were obtained at the M06/6-31G(d,p) and M06-L/D95V levels, respectively. The M06 level generally predicted a lower potential energy barrier for hydroxylation. These results clearly show that the hydrogen transfer reaction of the first step is rate-limiting.

3.3. Potential Energy Curves and the Dynamics of Hydrogen Transfer. The potential and vibrationally adiabatic energies along the hydrogen transfer coordinate were calculated at the M06/6-31G(d,p)/D95V level and are depicted in Figure 3. Changes in the $^{1}C-^{29}H$, $^{4}O-^{29}H$, and $^{1}C-^{4}O$ bond lengths

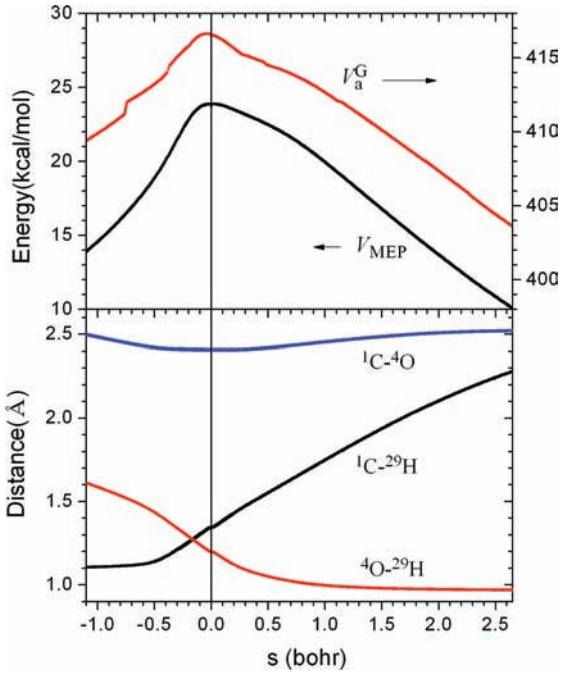

Figure 3. (top) Potential energy and adiabatic energy curves (black and red, respectively) and (bottom) bond lengths (as labeled) along the reaction coordinate for the hydrogen transfer, calculated at the M06/6-31G(d,p)/D95V level. The vertical line represents the position of the transition state TS1.

are also shown in Figure 3. The potential energy curve is smooth all along the reaction coordinate. The adiabatic curve has a small irregularity on the reactant side due to interpolation using the spline-under-tension fit. This irregularity does not have a big impact on the calculated results. Figure 3 shows that the $^{1}C-^{29}H$ bond length hardly changed from $s = -\infty$ to $s = -0.5$ but increased very rapidly for $s > -0.5$. The $^{4}O-^{29}H$ bond length decreased more rapidly for $s > -0.5$. These results demonstrate that from $s = -\infty$ to $s = -0.5$, heavy-atom motion brings the reaction centers closer. Hydrogenic motion becomes significant for $s > -0.5$. The $^{1}C-^{29}H$ and $^{4}O-^{29}H$ bond lengths crossed before $s = 0.0$, making the $^{1}C-^{29}H$ bond longer than the $^{4}O-^{29}H$ bond at TS1. This result indicates that TS1 occurs late along the reaction coordinate for the hydrogen transfer. This violates Hammond's postulate, which predicts an early TS when the reaction is exoergic.

Figure 4 depicts the changes in the Cu−N and Cu−O bonds along the reaction coordinate for the hydrogen transfer. It is

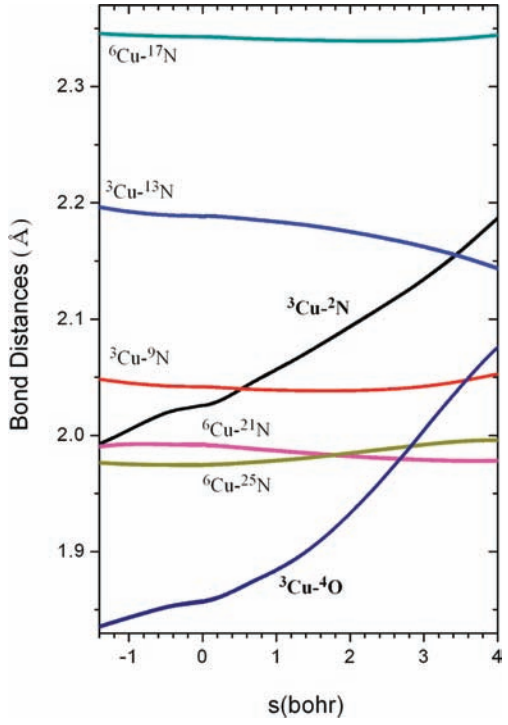

Figure 4. Cu−N and Cu−O bond distances along the reaction coordinate for the hydrogen transfer.

interesting that the $^{3}Cu-^{2}N$ bond length increased rapidly while other Cu−N bond lengths changed very little. This is likely attributable to the large positive charge on the ^{2}N atom due to breaking of the $^{1}C-^{29}H$ bond and formation of the $^{1}C-^{2}N$ double bond that occur in the hydrogen transfer reaction. As described earlier, this induces Coulomb repulsion with Cu. Figure 4 also shows that the $^{3}Cu-^{4}O$ bond breaks along the reaction coordinate for the hydrogen transfer. The formation of the $^{1}C-^{2}N$ double bond and the increased planarity of the methylene group due to breaking of the $^{1}C-^{29}H$ bond are depicted in Figure 5. The dihedral angle in Figure 5 became zero when the $^{1}C-^{29}H$ bond was completely broken in the intermediate. Both the $^{1}C-^{2}N$ bond length and the dihedral angle decreased suddenly at a very early stage of the $^{1}C-^{29}H$ bond breaking and then decreased smoothly with similar patterns afterward. Dihedral angle changes are related to the umbrella mode of vibration, which may be coupled with the reaction coordinate of the hydrogen transfer. It has been suggested that strong coupling between the umbrella mode and the hydrogen transfer reduces the primary KIE and increases the secondary KIE.[29] The slope of this angle around the TS, where the $^{1}C-^{29}H$ bond length was between 1.3 and 1.4 Å, was smaller than that when the bond length was larger than 1.4 Å. This result implies that mixing between the umbrella mode and the hydrogen transfer motion is not significant.

dx.doi.org/10.1021/ja211073t | J. Am. Chem. Soc. 2012, 134, 3524−3531

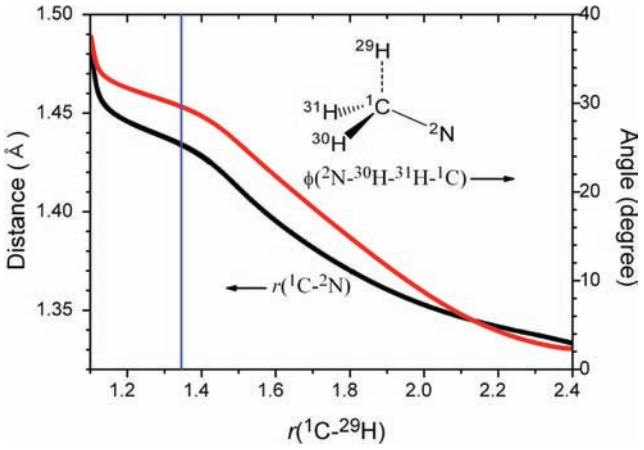

Figure 5. Variation of the $^{1}C-^{2}N$ bond distance and dihedral angle of the methylene group with breaking of the $^{1}C-^{29}H$ bond. The vertical line represents the location of the transition state for the hydrogen transfer.

3.4. Rate Constants, KIEs, and Tunneling. The rate constants and transmission coefficients were determined using CVT calculations with a semiclassical tunneling approximation. The results and the experimental rate constants are listed in Table 4. The tunneling effect is very significant, as indicated by the κ_H^{SCT} and κ_D^{SCT} values of 134 and 38, respectively, at 223 K. The calculated and experimental KIEs are listed in Table 5. The experimental KIE is 26.2 ± 2 at 233 K, whereas the calculated value with tunneling is 28.1. These values agree perfectly within the limits of experimental error. Without considering the tunneling effect, it would be impossible to reproduce the experimental results. The calculated and experimental Arrhenius plots are depicted in Figure 6. Although tunneling is significant in the hydrogen transfer, both the experimental and calculated Arrhenius plots are linear, probably because the temperature range is not large enough to see any curvature. The calculated plots had values below those of the experimental plots because the calculated rate constants were smaller than the experimental values. The calculated values of the Arrhenius activation energies for the hydrogen and deuterium transfers were E_a^H = 16.2 and E_a^D = 18.1 kcal/mol, respectively, both of which are larger than the corresponding experimental values by ~2.6 kcal/mol. The smaller rate constants and larger activation energies are probably due to the slightly overestimated potential energy barrier. The slightly higher potential energy barrier may originate from the difference between the C−H bond strengths for the methyl and isopropyl systems. The calculated values of $E_a^H - E_a^D$ and A_H/A_D were −1.86 kcal/mol and 0.51, respectively, which agree very well with the experimental values for the isopropyl system (−1.9 kcal/mol and 0.49, respectively). Solvent effect calculations for the activation potential energy of the hydrogen transfer were performed using the IEFPCM model[30] with THF solvent. However, the barrier height was almost the same as that of the gas-phase one.

Table 5. Calculated and Experimental H/D Kinetic Isotope Effects

T(K)	k_H^{CVT}/k_D^{CVT}	$\kappa_H^{SCT}/\kappa_D^{SCT}$	$k_H^{CVT/SCT}/k_D^{CVT/SCT}$	$(k_H/k_D)_{exptl}$
213	10.6	3.91	41.5	–
223	9.57	3.53	33.7	–
233	8.71	3.18	28.1	26.2 ± 2[a]
243	7.98	3.00	23.8	–
253	7.37	2.71	20.6	–
263	6.84	2.69	18.0	–

[a]For the isopropyl ligand in ref 4.

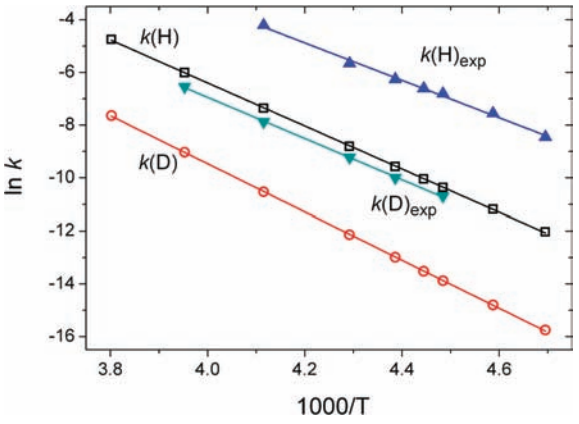

Figure 6. Arrhenius plots for the hydrogen and deuterium transfer reactions. Open and solid symbols denote predicted and experimental values, respectively.

The thermally weighted transmission coefficients are depicted in Figure 7, which shows that tunneling is significant even at energies far below the adiabatic energy maximum. The representative tunneling path (RTP)[31] is the one for which the thermally weighted transmission probability is maximized. It did not significantly depend on temperature over the range from 213 to 263 K. The RTP occurred when V_a^G = 413.0 kcal mol^{-1} at 213 K, which is ~3.6 kcal mol^{-1} below the top of the adiabatic energy barrier. Since the KIEs are very sensitive to the transmission probabilities, it is unlikely that the RTP was significantly misplaced. These results suggest that tunneling is very efficient for hydrogen transfer in the bis(μ-oxo)dicopper complex and that the RTP is very different from the MEP. These conclusions were also suggested by Shida et al.[32] and Kim.[33] The imaginary frequency at the transition state is not a crucial parameter in the dynamics of the hydrogen transfer because most reactive paths do not pass close to the transition

Table 4. Experimental[a] and Calculated Rate Constants (k, s^{-1}) and Transmission Coefficients (κ) for Hydrogen Transfer

T (K)	κ_H^{SCT}	$k_H^{CVT/SCT}$	k_H^{exptl}	κ_D^{SCT}	$k_D^{CVT/SCT}$	k_D^{exptl}
213	215	5.97×10^{-6}	–	55	1.44×10^{-7}	–
223	134	3.16×10^{-5}	5.72×10^{-3}	38	9.38×10^{-7}	–
233	89	1.50×10^{-4}	2.20×10^{-3}	28	5.34×10^{-6}	7.72×10^{-5}
243	63	6.38×10^{-4}	7.27×10^{-3}	21	2.68×10^{-5}	4.15×10^{-4}
253	46	2.46×10^{-3}	–	17	1.20×10^{-4}	1.22×10^{-3}
263	35	8.68×10^{-3}	–	13	4.83×10^{-4}	3.54×10^{-3}

[a]For the isopropyl ligand system in ref 4.

dx.doi.org/10.1021/ja211073t | J. Am. Chem. Soc. 2012, 134, 3524−3531

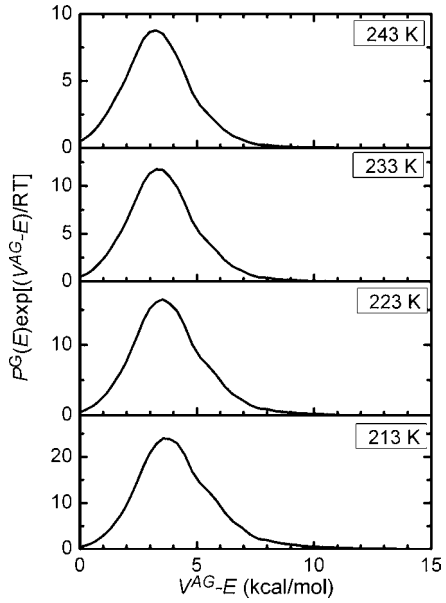

Figure 7. Thermally weighted transmission probability for the hydrogen transfer as a function of $V^{AG} - E$ at various temperatures, where V^{AG} is the adiabatic energy barrier maximum. The thermally weighted transmission probabilities are scaled by $\exp(V^{AG}/RT)$. It should be noted that $V^{AG} - E$ becomes larger as the total energy is reduced from the adiabatic energy barrier maximum.

state. Therefore, the one-dimensional tunneling model that uses the imaginary frequency as a key parameter may not be appropriate for a correct description of the hydrogen transfer in the bis(μ-oxo)dicopper complex. At 213 K, the pre- and post-tunneling configurations along the MEP occurred at s values of −0.54 and 0.94 bohr, respectively. Between these points, the hydrogen atom moved 0.57 Å by tunneling from ^{1}C to ^{4}O. At 233 K, the RTP occurred when V_a^G = 413.4 kcal/mol, which is 3.3 kcal/mol below the adiabatic energy maximum. The pre- and post-tunneling configurations occurred at s values of −0.47 and 0.85 bohr, respectively. The hydrogen hopped 0.54 Å by tunneling. In the conversion of the bis(μ-oxo)dicopper complex to the configuration of the RTP, the distance between the ^{1}C and ^{4}O atoms was reduced by 0.48 Å while the bonding ^{1}C−^{29}H distance was increased by only 0.039 Å. Thus, it is mainly heavy atoms that move as the reaction progresses from the reactant complex to the pretunneling configuration. At that point, the hydrogen atom hops. These results suggest that tunneling is very efficient for the hydrogen transfer of the bis(μ-oxo)dicopper complex and that the RTP is very different from the MEP.

4. CONCLUDING REMARKS

Many biological enzymes that contain metal ions such as copper and iron perform their enzymatic functions by a hydrogen transfer process. To understand the role of the metal core center in these enzymatic actions, several model systems that mimic natural enzyme functions have been developed by reducing the size of the natural enzymes to a chemically manageable level. The models have then been tested for their catalytic activity. A dicopper enzyme model system that activates C−H bonds by a hydrogen transfer from the substrate to the catalytic dicopper center exhibited exceptionally large KIE values. This indicates a significant tunneling effect for the hydrogen transfer path. In this work, we first demonstrated that accurate prediction of KIE and Arrhenius parameters in such model systems is possible in practice using variational transition state theory including a multidimensional tunneling approximation based on state-of-the-art quantum-mechanical calculations for the hydrogen transfer intrinsic reaction path.

The experimental KIE is 26.2 ± 2 at 233 K, whereas the value calculated with tunneling is 28.1. These two values agree perfectly within the limits of experimental error. The calculated values of $E_a^H - E_a^D$ and A_H/A_D were −1.86 kcal/mol and 0.51, respectively, which agree very well with the experimental values for the isopropyl system (−1.9 kcal/mol and 0.49, respectively). We found that tunneling is very efficient for the hydrogen transfer in the bis(μ-oxo)dicopper complex and that the RTP is very different from the MEP. At 233 K, the RTP occurs when V_a^G is 3.3 kcal/mol below the adiabatic energy maximum. The pre- and post-tunneling configurations occur at s values of −0.47 and 0.85 bohr, respectively, where the actual distance that the hydrogen travels by tunneling is 0.54 Å. It is mainly heavy atoms that move as the reaction proceeds from the reactant complex to the pretunneling configuration. At that point, the hydrogen atom suddenly hops.

■ ASSOCIATED CONTENT

Supporting Information

Complete refs 25 and 26. This material is available free of charge via the Internet at http://pubs.acs.org.

■ AUTHOR INFORMATION

Corresponding Author

ypak@pusan.ac.kr; yhkim@khu.ac.kr

Notes

The authors declare no competing financial interest.

■ ACKNOWLEDGMENTS

This research was supported in part by the Basic Science Research Program through the National Research Foundation (NRF) of Korea funded by the Ministry of Education, Science and Technology (Grant 2010-0012990). We are pleased to acknowledge the support of the Center for Academic Computing at Kyung Hee University for computing resources. The authors thank Professor Donald G. Truhlar (Department of Chemistry, University of Minnesota) for the Polyarte and Gaussrate programs.

■ REFERENCES

(1) Solomon, E. I.; Sundaram, U. M.; Machonkin, T. E. *Chem. Rev.* **1996**, *96*, 2563.
(2) Hatcher, L. Q.; Karlin, K. D. *J. Biol. Inorg. Chem.* **2004**, *9*, 669.
(3) Bento, I.; Carrondo, M. A.; Lindley, P. F. *J. Biol. Inorg. Chem.* **2006**, *11*, 539.
(4) Mahapatra, S.; Halfen, J. A.; Tolman, W. B. *J. Am. Chem. Soc.* **1996**, *118*, 11575.
(5) Whittaker, M. M.; Ballou, D. P.; Whittaker, J. W. *Biochemistry* **1998**, *37*, 8426.
(6) Que, L. Jr.; Tolman, W. L. *Angew. Chem., Int. Ed.* **2002**, *41*, 1114.
(7) Cramer, C. J.; Pak, Y. *Theor. Chem. Acc.* **2001**, *105*, 477.
(8) Cramer, C. J.; Kinsinger, C. R.; Pak, Y. *THEOCHEM* **2003**, *632*, 111.
(9) Garrett, B. C.; Truhlar, D. G.; Grev, R. S.; Magnuson, A. W. *J. Phys. Chem.* **1980**, *84*, 1730.
(10) Truhlar, D. G.; Garrett, B. C. *Acc. Chem. Res.* **1980**, *13*, 440.
(11) Liu, Y. P.; Lynch, G. C.; Truong, T. N.; Lu, D. H.; Truhlar, D. G.; Garrett, B. C. *J. Am. Chem. Soc.* **1993**, *115*, 2408.
(12) Truhlar, D. G.; Garrett, B. C. *J. Chem. Phys* **1987**, *84*, 365.

(13) Truhlar, D. G.; Isaacson, A. D.; Garrett, B. C. In *Theory of Chemical Reaction Dynamics*; Baer, M., Ed.; CRC Press: Boca Raton, FL, 1985.
(14) Truhlar, D. G.; Liu, Y.-P.; Schenter, G. K.; Garrett, B. C. *J. Phys. Chem.* **1994**, *98*, 8396.
(15) Stephens, P. J.; Devlin, F. J.; Chabalowski, C. F.; Frisch, M. J. *J. Phys. Chem.* **1994**, *98*, 11623.
(16) Zhao, Y.; Truhlar, D. G. *Theor. Chem. Acc.* **2008**, *120*, 215.
(17) Zhao, Y.; Truhlar, D. G. *J. Chem. Phys.* **2006**, *125*, No. 194101.
(18) Perdew, J. P.; Burke, K.; Ernzerhof, M. *Phys. Rev. Lett.* **1996**, *77*, 3865.
(19) Hay, P. J.; Wadt, W. R. *J. Chem. Phys.* **1985**, *82*, 270.
(20) Dunning, T. H., Jr.; Hay, P. J. In *Modern Theoretical Chemistry*; Schaefer, H. F., III, Ed.; Plenum: New York, 1976; Vol. 3, p 1.
(21) Valero, R.; Costa, R.; Moreira, I. d. P. R.; Truhlar, D. G.; Illas, F. *J. Chem. Phys.* **2008**, *128*, No. 114103.
(22) Baldridge, K. K.; Gordon, M. S.; Steckler, R.; Truhlar, D. G. *J. Phys. Chem.* **1989**, *93*, 5107.
(23) Corchado, J. C.; Coitiño, E. L.; Chuang, Y.-Y.; Fast, P. L.; Truhlar, D. G. *J. Phys. Chem. A* **1998**, *102*, 2424.
(24) Corchado, J. C.; Chuang, Y.-Y.; Coitio, E. L.; Ellingson, B. A.; Zheng, J.; Truhlar, D. G. *Gaussrate*, version 9.7; University of Minnesota: Minneapolis, MN, 2007.
(25) Frisch, M. J.; et al. *Gaussian 03*, revision E; Gaussian, Inc.: Wallingford, CT, 2004.
(26) Corchado, J. C.; et al. *Polyrate*, version 9.7; University of Minnesota: Minneapolis, MN, 2007.
(27) Fast, P. L.; Corchado, J. C.; Truhlar, D. G. *J. Chem. Phys.* **1998**, *109*, 6237.
(28) Fast, P. L.; Truhlar, D. G. *J. Chem. Phys.* **1998**, *109*, 3721.
(29) Huskey, W. P.; Schowen, R. L. *J. Am. Chem. Soc.* **1983**, *105*, 5704.
(30) Tomasi, J.; Mennucci, B.; Cammi, R. *Chem. Rev.* **2005**, *105*, 2999.
(31) Kim, Y.; Truhlar, D. G.; Kreevoy, M. M. *J. Am. Chem. Soc.* **1991**, *113*, 7837.
(32) Shida, N.; Barbara, P. F.; Almlof, J. *J. Chem. Phys.* **1991**, *94*, 3633.
(33) Kim, Y. *J. Am. Chem. Soc.* **1996**, *118*, 1522.
(34) Mahapatra, S.; Halfen, J. A.; Wilkinson, E. C.; Pan, G.; Wang, X.; Young, V. G. J.; Cramer, C. J.; Que, L. J.; Tolman, W. B. *J. Am. Chem. Soc.* **1996**, *118*, 11555.